High power impulse magnetron sputtering discharges: Instabilities and plasma self-organization

EHIASARIAN, Arutiun <http://orcid.org/0000-0001-6080-3946>, HECIMOVIC, A., DE LOS ARCOS, T., NEW, Roger, DER GATHEN, V. Schulz-von, BOKE, M. and WINTER, J.

Published version

EHIASARIAN, Arutiun, HECIMOVIC, A., DE LOS ARCOS, T., NEW, Roger, DER GATHEN, V. Schulz-von, BOKE, M. and WINTER, J. (2012). High power impulse magnetron sputtering discharges: Instabilities and plasma self-organization. Applied Physics Letters, 100 (11), p. 114101.

High power impulse magnetron sputtering discharges: Instabilities and plasma self-organization

A. P. Ehiasarian, A. Hecimovic, T. de los Arcos, R. New, V. Schulz-von der Gathen et al.

Citation: Appl. Phys. Lett. **100**, 114101 (2012); doi: 10.1063/1.3692172
View online: http://dx.doi.org/10.1063/1.3692172
View Table of Contents: http://apl.aip.org/resource/1/APPLAB/v100/i11
Published by the American Institute of Physics.

High power impulse magnetron sputtering discharges: Instabilities and plasma self-organization

A. P. Ehiasarian,[1,a)] A. Hecimovic,[2] T. de los Arcos,[2] R. New,[1] V. Schulz-von der Gathen,[2] M. Böke,[2] and J. Winter[2]
[1]*HIPIMS Technology Centre, Sheffield-Hallam University, Sheffield, United Kingdom*
[2]*Institute of Experimental Physics II, Ruhr-University Bochum, Germany*

(Received 21 July 2011; accepted 15 February 2012; published online 12 March 2012)

We report on instabilities in high power impulse magnetron sputtering plasmas which are likely to be of the generalized drift wave type. They are characterized by well defined regions of high and low plasma emissivity along the racetrack of the magnetron and cause periodic shifts in floating potential. The azimuthal mode number m depends on plasma current, plasma density, and gas pressure. The structures rotate in $\vec{E} \times \vec{B}$ direction at velocities of $\sim$10 km s^{-1} and frequencies up to 200 kHz. Collisions with residual gas atoms slow down the rotating wave, whereas increasing ionization degree of the gas and plasma conductivity speeds it up. © *2012 American Institute of Physics*. [http://dx.doi.org/10.1063/1.3692172]

High power impulse magnetron sputtering (HIPIMS) is the latest innovation in physical vapor deposition technology.[1] It combines high voltage/high current impulse glow discharges with conventional magnetron cathodes to achieve a highly ionized sputtered flux. At peak powers of kW cm^{-2}, heat flux management at the cathode is achieved by pulsing at low duty cycle with typical durations of a few 100 μs and frequencies of a few 100 Hz. The deposition environment of HIPIMS has characteristic high surface adatom mobility and can produce highly adherent[2] and fully dense thin films.[3]

The HIPIMS plasma discharge is often reported to be homogeneous, however perfect homogeneity is seldom observed in discharges in general. For example, unmagnetized high power DC glow discharges self-organize in structures of modulated intensity at the cathode.[4] The mere presence of a magnetic field in finite plasma with density gradients promotes plasma instabilities.[5] Moreover, the high discharge current density in HIPIMS plasmas of the order of several A cm^{-2} and the presence of crossed electric and magnetic fields induce a strong azimuthal $\vec{E} \times \vec{B}$ drift.[6–8]

Magnetrons confine (magnetize) electrons, whereas ion loss rates are high. This may give rise to two-stream instabilities that occur due to large differences in fluxes of electrons and ions.[8,9]

Several drift wave type instabilities have been classified in Hall thrusters[10] whose configuration is topologically similar to HIPIMS. Recent fast-frame photography has shown that indeed HIPIMS plasmas exhibit striations—faint bands with alternating low and high intensity—in a direction perpendicular to the $\vec{E} \times \vec{B}$ drift.[11]

In this contribution, we report the observation of centimeter-size, well-defined bright and dark regions of plasma arranged periodically along the full length of the racetrack of a circular HIPIMS magnetron. As will be shown, these features resemble the footprint of drift-wave lobes with well defined azimuthal periodicity, i.e., mode number m. They rotate with frequencies of the order of 100 kHz and velocities of $\sim$10 km s^{-1}.

Experiments were conducted at Ruhr-University, Bochum, in a UHV cylindrical vacuum chamber of 45 cm height and 35 cm diameter, pumped by a turbomolecular pumping system to a base pressure of 1×10^{-6} mbar. We employed a standard circular magnetron with a field created by a single cylindrical magnet acting as the inner pole and a monolithic ring magnet as the outer pole. The cathode was furnished with a Ti target with a diameter of 50 mm and an area of 20 cm^2. The maximum tangential magnetic field strength on the target surface was 60 mT measured 2 mm above the race track. The inner pole was south and the outer pole was north resulting in an $\vec{E} \times \vec{B}$ drift in anticlockwise direction, as illustrated in Fig. 1. The discharge was driven by a HMP 2/1 generator (Huettinger Electronic). Typical peak pulse parameters were current of 90 A, voltage of -700 V, duration of 200 μs, and frequency of 20 Hz.

To study the discharge with high temporal- and spatial resolution, we observed the cathode surface face-on through a silica glass view port with wavelength cutoff at 300 nm. The window retained transparency over a period of 20 operation hours. Fast photography was realized using a single shot camera type PIMAX 1024 (Princeton Instruments) with image intensifier, equipped with a UV-Nikkor 105 mm f 1:4.5 objective. The camera exposure was synchronized with the discharge pulses and the CCD detector was gated for 150 ns through an electronic shutter. The gate width was chosen to be shorter than the characteristic motion time of the observed structures, in particular exposures of 30, 70, 150, and 300 ns revealed no change in the localization of the structures, whereas longer exposures of 1000 and 2000 ns showed significant smearing of the image. With the shutter closed, the detector picked up a constant background of $\sim$1% of the maximum intensity, which was subtracted from the images.

Fig. 2 shows images of the race track (total light) emission at different peak current densities (J_d) and argon pressure (P_{Ar}). At low currents, the plasma is essentially homogeneously

a)Author to whom correspondence should be addressed. Electronic mail: A.Ehiasarian@shu.ac.uk.

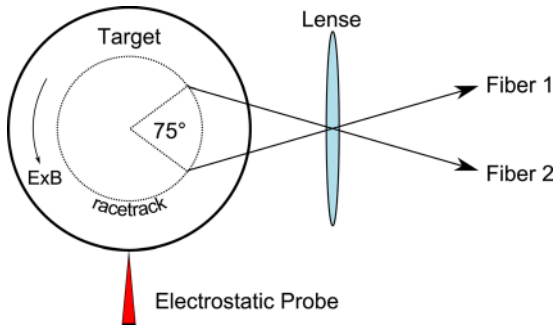

FIG. 1. (Color online) Unfolded view of the target with arrangement of Langmuir probe and local optical measurement. The actual light paths were in a plane perpendicular to the target.

distributed around the race track (Fig. 2(a)). However, due to the low emission intensity from the plasma, we cannot fully exclude the existence of discrete structures on the surface with a very high mode number, i.e., consisting of many (>50) merging lobes. At high currents (Figs. 2(b) and 2(f)), there is one distinct region of low intensity. At high pressures (Figures 2(c), 2(d), 2(g), 2(h)), we recognize three and four distinct structures with similar appearance and size.

In Fig. 2(b), following the intensity in the direction of $\vec{E} \times \vec{B}$ drift, i.e., counter clockwise around the race track, we observe that the periodicity starts with a stepwise increase in intensity followed by gradual increase to a maximum and a gradual reduction. This is also observed in Fig. 2(d) for each of the four structures.

The floating potential with respect to ground was measured using a single Langmuir probe with length of 5 mm and diameter of 50 μm, positioned at a height of 19 mm above the magnetron surface and a radial distance of 25 mm from the magnetron centre (Fig. 1).

The local intensity of total light from two well defined points on the target was imaged onto two photomultipliers (PMT) and recorded independently (Fig. 1). The optical foci were put at the position of the racetrack above the target surface at an angular distance of 75° and linear distance of 20 mm with respect to the racetrack centerline. The points were selected by projecting an image of the target onto two fiber optic cables positioned at the focal length of a single lens, as shown in Fig. 1. Their diameter in the focal plane is estimated to be about 1 mm. The direction of motion of plasma features was inferred from the phase shift between PMT signals. The speed of motion was calculated from the time shift and the distance between observed points. The frequency of rotation was obtained from Fast Fourier Transform (FFT) analysis.

Signals from the individual optical fibers and of the floating potential as a function of time are given in Fig. 3. All signals have the same well-defined periodicity. The structures are stable and maintain constant amplitude, frequency, and wavelength within the observed time period as confirmed by FFT (not shown) spectra which consisted of a well-defined peak at a characteristic frequency and clearly present second and third order harmonics. This is characteristic of a saturated drift mode type instability.[12,13] At other parameters, multiple frequencies and even chaotic states may be observed. This will be analyzed in detail in further investigations.

The trace of the floating potential, Fig. 3, was measured in a region of expanding remote plasma streaming radially away from the cathode. The minima in the signal can be interpreted as an increase in electron density, and therefore correlate with PMT maxima due to increase in the excitation and emission in the part of the plasma with elevated electron density.

The observed behavior may be due to particle beams emitted from the rotating structures like a beacon and/or due to a modulation of the electron temperature in this region. The exact nature of this modulation of the floating potential and the connection to light intensity is still unclear and under investigation. The sheer magnitude of the changes in floating potential implies that they are caused by large fluxes of particles and/or considerable changes in plasma temperature.

Comparing the signals from the two optical fibers as shown in Fig. 3, we observe a time shift of 1.3 μs. Using recognizable features and varying the angle between the two

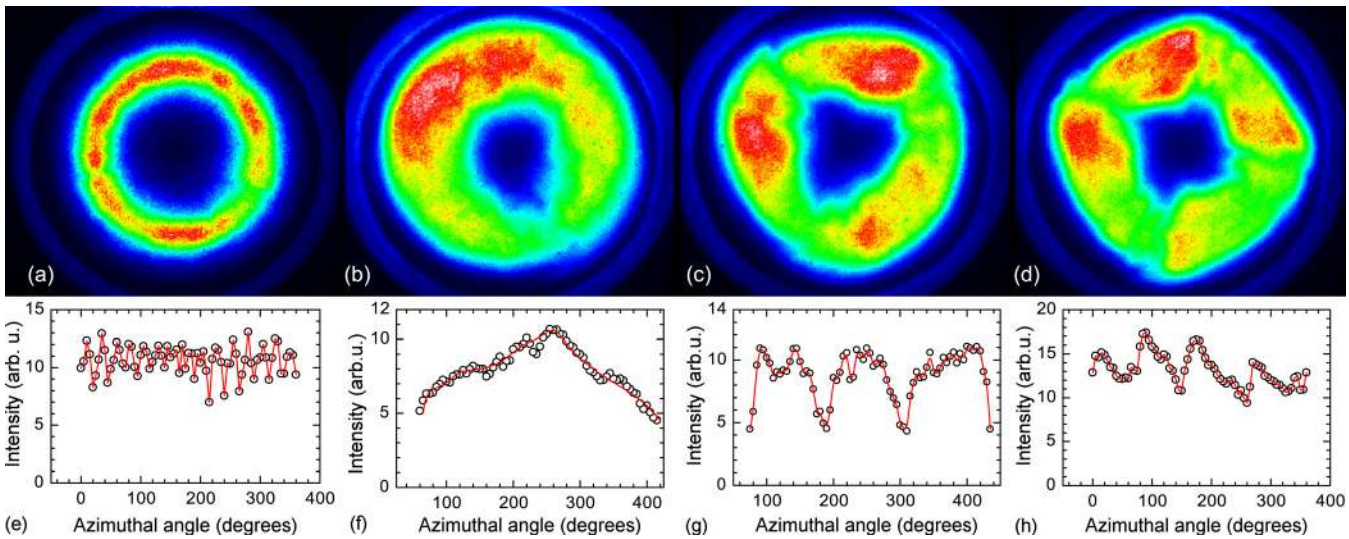

FIG. 2. (Color online) Influence of peak current density and Ar pressure on the discharge: (a) and (e) $J_d = 0.75$ A cm^{-2}, $P_{Ar} = 0.17$ Pa; (b) and (f) $J_d = 7.5$ A cm^{-2}, $P_{Ar} = 0.17$ Pa; (c) and (g) $J_d = 7.5$ A cm^{-2}, $P_{Ar} = 1.0$ Pa; and (d) and (h) $J_d = 7.5$ A cm^{-2}, $P_{Ar} = 1.7$ Pa. Upper row: fast photography frames (false color), lower row: total light intensity vs azimuthal angle corresponding to a circle along the centre of the racetrack. Angle is counted clockwise.

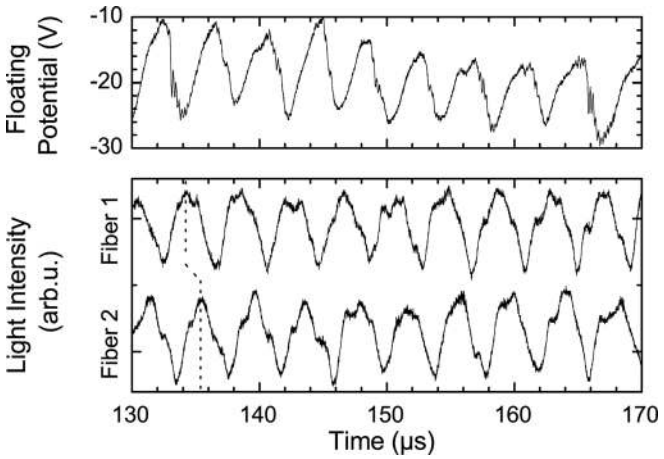

FIG. 3. Signals from optical fibers and the floating potential measured by electrostatic probe at $J_d = 7.5\,\mathrm{A\,cm^{-2}}$, $P_{Ar} = 1.7\,\mathrm{Pa}$. Corresponding features in both fibers are marked with a dotted line.

fibers, we found that the phase shift is in positive direction indicating that the periodic structures move anticlockwise along the track following the direction of $\vec{E} \times \vec{B}$ drift expected for this cathode. The linear speed of motion is in the range 10–20 km s^{-1}. Thus, the PMT signals in conjunction with the camera images show unambiguously that there is a wave of particles propagating through the plasma in the direction of the $\vec{E} \times \vec{B}$ drift responsible for excitation of atoms.

The experimental values for frequency and time shift obtained from PMT measurements were used to calculate velocity (u), wavelength (λ), and expected number of lobes within the circumference of the racetrack (Table I). The correlation between the number of features calculated from the PMT signals and actual number of features observed in camera shots in Figs. 2(b)–2(d) is very good.

The parameters of the rotating lobes are strongly influenced by the pressure P_{Ar} (Table I). The experimental data suggests that there is an inverse relation between velocity and pressure. Since the frequency of collisions in the plasma is proportional to the density, $\nu = n\sigma v$ (Ref. 5) and making use of the gas state $P_{Ar} = n_{Ar} k T_{Ar}$ we can conclude that as the pressure increases the density of Ar atoms is elevated consequently increasing the collision frequency and decreasing the rotation speed of the instability. This indicates collisional slowing down of the wave.

Two separate experiments have demonstrated a link between wave velocity, u, and plasma conductivity, σ.

A linear relationship between wave velocity and peak current density, J_d, was observed and approximated by

TABLE I. Influence of gas pressure at a peak current of 150 A (7.5 A cm^{-2}) on the parameters of the rotating structures. The wavelength was calculated by dividing velocity by frequency.

P_{Ar} (Pa)	Freq. (kHz)	Time shift (μs)	u (km s^{-1})	λ (mm)	No. of waves in racetrack	No. of observed features
0.16	188	1.39	15.0	79.7	1.25	1
1.0	368	1.57	13.3	36.1	2.8	3
1.65	445	1.85	11.3	25.3	4	4

$$u(\mathrm{kms^{-1}}) = 1.28 J_d + 8.2 \sim n_{pl}, \tag{1}$$

where n_{pl} is the plasma density. Previous contributions[14] have shown an increase in plasma density and ionization degree with discharge current, therefore in Eq. (1), we can substitute discharge current with plasma density.

When operating at a reduced tangential magnetic field strength on the cathode surface (accomplished by increasing the thickness of the target), we observed that a factor 1.5 decrease in magnetic induction (from 136 to 88 mT) boosted wave velocity by a factor of 2.5 (from 15 to 35 km s^{-1}). Tangential B-fields are known to limit diffusion and diminish plasma conductivity.[5]

To understand the observed dependences, we take into account that the observed wave motion is in an $\vec{E} \times \vec{B}$ direction and examine the expression for conductivity of electrons perpendicular to the electric and magnetic field, i.e., Hall conductivity,[16]

$$\sigma_H = \frac{\omega_c \nu_c}{\omega_c^2 + \nu_c^2} \frac{n_e e^2}{m_e \nu_c}, \tag{2}$$

where ω_c is electron cyclotron frequency, ν_c is electron collision frequency, n_e is electron density, and m_e is the electron mass. In the present experiment, $\omega_c \sim 10\,\mathrm{GHz}$ is much higher than $\nu_c \sim 50\,\mathrm{MHz}$. Introducing the approximation $\omega_c \gg \nu_c$ in Eq. (2) and replacing $\omega_c = eB/m_e$, we derive the following equation:

$$\sigma_H = \frac{n_e e}{B}. \tag{3}$$

Equation (3) shows that Hall conductivity is proportional to the electron density, which is equivalent to plasma density due to quasineutrality of the plasma, and inversely proportional to the magnetic field. This allows to interpret the observed increase in wave velocity with plasma density as a result of increased conductivity of the plasma in the direction of wave movement. Reducing the tangential magnetic field increases Hall conductivity resulting in the observed increase of wave velocities. Physically, this means that increasing the density of charged particles provides a better conducting media for wave propagation; similarly, reducing magnetic field strength reduces confinement (increases Larmour radius), enhances diffusivity, and allows faster wave propagation.

The frequency of the waves is between 100 and 200 kHz, and is considerably smaller than the lower hybrid frequency which is of the order of 2 MHz.[9] We cannot exclude at this stage that there might be faint high frequency components superimposed on the wave patterns, which could be indicative of two stream instabilities as discussed by Böhlmark *et al.*[15] and Lundin *et al.*[9]

The wavelength increases with peak current of the discharge indicating that energy input, calculated as the product of current, voltage and time, results in a stronger driving force which would stabilize the periodicity. The wavelength also increased at lower gas density, where the energy dissipation ability of the environment is reduced, therefore, allowing instabilities to be sustained at lower energy input.

Magnetosonic waves, characterized by a propagation in $\vec{E} \times \vec{B}$ direction, would exhibit similar wavelengths to the ones observed (Table I) for magnetic field of 5 mT and plasma density $10^{16}\,\mathrm{cm}^{-3}$, which are values close to those in the dense plasma region ~1 cm above the target. They also predict that at low density, the wavelength extends beyond the length of the racetrack. However, they and Alfven waves, being hydromagnetic waves, predict a reduction in velocity with density, which appears to contradict our experiment.

The exact nature of the observed instability is still unclear. The magnetic topology in these experiments is more complex than in, e.g., simple drift wave experiments in cylindrical plasmas confined by co-axial homogeneous magnetic fields.[12,13]

Following our conclusion that the instability rotation direction corresponds to the drift direction generated by the $\vec{E} \times \vec{B}$ drift and the finding by Choueri[10] that instabilities in Hall thrusters, where plasma parameters are comparable to HIPIMS plasma parameters, are high frequency azimuthal drift waves, we can conclude that our observed waves are of the generalized $\vec{E} \times \vec{B}$ drift wave type.

In summary, our observations clearly demonstrate that HIPIMS plasma is a highly complex and inhomogeneous form of plasma discharge. The phenomena observed and presented in this paper are most probably drift wave instabilities. Under certain experimental conditions, the instabilities saturate and result in structures with various azimuthal periodicity (*m*-number) rotating at frequencies between 100 kHz and 200 kHz. The rotation speed is slowed down by collisions with the residual gas and is dependent on the conductivity of the medium. The instabilities result in intermittent enhanced particle transport away from the cathode which may be of significant technological importance. The nature and properties of these particle fluxes still have to be investigated. It may be speculated that the observed modulated floating potential may be due to particle beams (beacons) emitted outwards from the cathode area.

This work was supported by DFG within SFB TR 87 Project and by the Research Department "Plasmas with complex Interactions" of Ruhr-University Bochum.

[1]V. Kouznetsov, K. Macak, J. M. Schneider, U. Helmersson, and I. Petrov, Surf. Coat. Technol. **122**(2), 290 (1999).
[2]A. P. Ehiasarian, J. G. Wen, and I. Petrov, J. Appl. Phys. **101**, 054301 (2007).
[3]A. P. Ehiasarian, A. Vetushka, Y. Aranda Gonzalvo, L. Szekely, G. Safran, and P. Barna, J. Appl. Phys. **109**, 104314 (2011).
[4]M. S. Benilov, Phys. Rev. E **77**(3), 036408 (2008).
[5]F. F. Chen, *Introduction to Plasma Physics* (Plenum, New York, 1984), p. 199.
[6]S. M. Rossnagel and H. R. Kaufman, J. Vac. Sci. Technol. **A5**(1), 88 (1987).
[7]A. Vetushka and J. W. Bradley, J. Phys. D: Appl. Phys. **40**(7), 2037 (2007).
[8]N. Brenning, I. Axnäs, M. A. Raadu, D. Lundin, and U. Helmersson, Plasma Sources Sci. Technol. **17**(4), 045009 (2008).
[9]D. Lundin, P. Larsson, E. Wallin, M. Lattemann, N. Brenning, and U. Helmersson, Plasma Sources Sci. Technol. **17**(3), 035021 (2008).
[10]E. Y. Choueri, Phys. Plasmas **8**, 1411 (2001).
[11]A. P. Ehiasarian, in *Plasma Surface Engineering Research and its Practical Applications*, edited by R. Wei (Research Signpost, Kerala, India, 2008), pp. 35–86.
[12]W. Biel, H. Kempkens, and J. Uhlenbusch, Plasma Phys. Controlled Fusion **40**, 1845 (1998).
[13]S. Klose, W. Bohmeyer, M. Laux, H. Meyer, G. Fussmann, and the PSI-team, Contrib. Plasma Phys. **41**, 467 (2001).
[14]A. P. Ehiasarian, A. Vetushka, A. Hecimovic, and S. Konstantinidis, J. Appl. Phys. **104**(8), 083305 (2008).
[15]J. Bohlmark, U. Helmersson, M. VanZeeland, I. Axnäs, J. Alami, and N. Brenning. Plasma Sources Sci. Technol. **13**, 654 (2004).
[16]A. Piel, *Plasma Physics: An Introduction to Laboratory, Space, and Fusion Plasmas* (Springer, Berlin, 2010).